Physica Scripta. Vol. T59, 352–359, 1995

Nonneutral Ion Plasmas and Crystals in Penning Traps*

J. J. Bollinger, Joseph N. Tan, Wayne M. Itano and D. J. Wineland

Time and Frequency Division, NIST, Boulder, CO 80303, U.S.A.

and

D. H. E. Dubin

Department of Physics, University of California at San Diego, La Jolla, CA 92093, U.S.A.

Received September 25, 1994; accepted December 15, 1994

Abstract

Experimental work which uses laser-cooled ions in Penning traps is reviewed. With laser-cooling the ions are strongly coupled and exhibit spatial correlations characteristic of a liquid or crystal. In plasmas with dimensions less than 10–15 interparticle spacings, the observed correlations are strongly affected by the finite size and shape of the trapping potential. Plasmas with greater than 60 interparticle spacings should exhibit correlations characteristic of an infinite one-component plasma. Radiation pressure from a laser is also used to apply a torque to the plasma and change the plasma density. This permits access to all possible thermal equilibria, including the maximum density state where the plasma undergoes Brillouin flow. If the size of the plasma is small compared to the trap dimensions, Penning traps produce plasmas with simple shapes whose normal modes can be calculated exactly. The modes provide a nondestructive diagnostic technique for obtaining information on the plasma density and shape.

1. Introduction

Ions in a trap form a nonneutral plasma when the ion density is sufficiently high or the ion temperature sufficiently low that the Debye length λ_D (see Section 2) is small compared to the ion cloud dimensions [1, 2]. This paper reviews some of the properties of ion plasmas in a Penning trap. Because Paul or r.f. (radio frequency) trap plasmas can be considered to be special cases of Penning trap plasmas (see Section 2), the general discussion can be applied to r.f. traps as well. Throughout the paper we will give experimental examples from measurements done on plasmas of laser-cooled $^9Be^+$ ions in a Penning trap. Laser-cooling makes it easy to satisfy the inequality $\lambda_D \ll$ plasma dimensions. However, cooling with a room temperature buffer gas has also been used to obtain λ_D much less than the plasma dimensions in some r.f. trap experiments [3].

Section 2 reviews the static, thermal equilibrium properties of cold Penning trap plasmas. The plasmas have a uniform density and, if the plasma dimensions are small compared to the trap dimensions, have the simple shape of a spheroid. The aspect ratio of the spheroid can be related to the ion density and parameters of the trap. Section 3 discusses the correlated behavior of the ions, which occurs when the ion thermal energy is small compared to the potential energy between nearest neighbor ions. This state can be obtained with laser-cooling. In small ion plasmas the spatial correlations have been observed using imaging techniques. Recently, Bragg scattering has been used to obtain information on the correlations when imaging techniques were no longer possible. Section 4 describes how radiation pressure from lasers can be used to apply a torque to a Penning trap plasma and increase the ion density. When axial asymmetries in the trap are minimized, it is possible to obtain the maximum density state allowed under thermal equilibrium, sometimes called the Brillouin limit. Section 5 discusses the electrostatic plasma modes of Penning trap plasmas. In the limit that the plasmas have uniform densities and spheroidal shapes, these modes can be calculated exactly. The modes provide a nondestructive diagnostic technique for obtaining information on the plasma shape and density. This should be useful in experiments where fluorescence techniques are not available, such as in antimatter experiments where current techniques to obtain diagnostic information involve dumping the plasma out of the trap. The modes can also resonantly enhance trap asymmetries and set limits to the density that can be obtained in Penning traps.

2. Static properties

The Penning trap shown in Fig. 1 consists of four cylindrical electrodes. The outer cylinders are called the "endcap" electrodes in analogy with the endcaps of a hyperbolic Penning trap [4]. The inner cylinders are electrically shorted and together called the "ring" electrode. With a positive potential V_T applied to the endcap electrodes with respect to the ring electrode, positively charged particles (ions) can be electrostatically confined in the direction of the trap axis. A static, uniform magnetic field $\boldsymbol{B} = B\hat{\boldsymbol{z}}$ parallel to the trap's symmetry axis confines the ions in the radial direction. Near the center of the trap, where the ions are confined, the radial component of the trap electric field is directed outward. This field produces an $\boldsymbol{E} \times \boldsymbol{B}$ circular drift of the ions about the symmetry axis of the trap. As the ions rotate through the magnetic field, they experience a Lorentz force directed radially inward.

With long enough confinement, the ions evolve to a state of thermal equilibrium where the rotation of the ions about the magnetic field axis is uniform or "rigid" at a frequency ω_r [5–7]. Specifically, the rotation frequency ω_r is independent of the radial position of an ion in the plasma. In the limit of zero temperature, the plasma density n_0 is constant

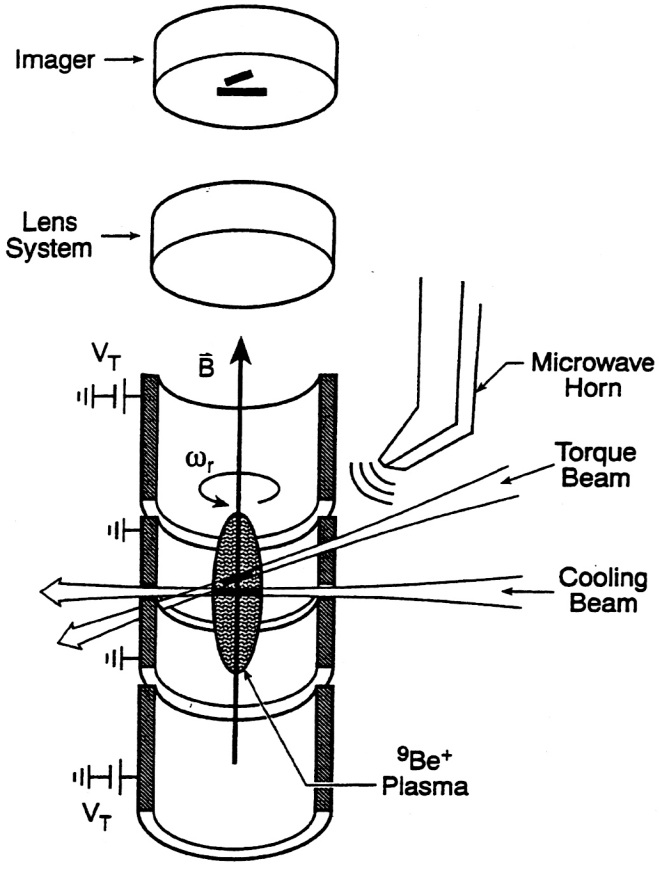

Fig. 1. Sketch of a Penning trap used to trap plasmas of Be^+ ions. The size of the plasma is exaggerated. The trap electrodes are right circular cylinders with an inner radius of 1.27 cm. They provide a quadratic potential near the trap center. Work was done with B ranging from 0.82 T to 6 T and V_T ranging from 10 V to about 1.5 kV (at 6 T). For $^9Be^+$ ions this gives a cyclotron frequency ranging from 1.4 MHz to 10 MHz and a trap axial frequency ranging from 125 kHz to 1.54 MHz.

in the plasma interior and drops abruptly to 0 at the plasma edge. The density depends on the rotation frequency according to (SI units are used throughout)

$$n_0 = 2\varepsilon_0 m\omega_r(\Omega - \omega_r)/q^2, \tag{1}$$

where $\Omega = qB/m$ is the ion cyclotron frequency, q and m are the charge and mass of the ion, and ε_0 is the permittivity of vacuum. Nonneutral plasmas exhibit collective effects such as plasma waves just like neutral plasmas. The plasma frequency ω_p is a function of the plasma density and is therefore related to the rotation frequency through the equation

$$\omega_p^2 \equiv \frac{q^2 n_0}{\varepsilon_0 m} = 2\omega_r(\Omega - \omega_r). \tag{2}$$

In this paper we use the convention that the symbols ω_r and Ω denote positive quantities. However, for positive ions, the sense of the rotation and the sense of the cyclotron motion with respect to $\boldsymbol{B}$ are actually negative. Specifically, when viewed from above the x–y plane, the ions move in clockwise orbits. For nonzero temperatures, the density drops to 0 at the plasma edge in a distance on the order of a Debye length λ_D [5, 7], where

$$\lambda_D = \left[\frac{\varepsilon_0 kT}{n_0 q^2}\right]^{1/2}, \tag{3}$$

k is Boltzmann's constant, and T is the ion temperature. When λ_D is much less than the plasma dimensions, the plasma therefore has a uniform density, given by eq. (1), with sharp boundaries. For very low temperatures, there are correlations in the ion positions [8–10] (see Section 3), and the ion density is not constant over length scales small compared to the inter-ion spacing ($\sim n_0^{-1/3}$). However, as long as the inter-ion spacing is small compared to the plasma dimensions (this is, as long as the number of ions $N \gg 1$), the plasma can be treated as a constant-density plasma for many problems. Two examples are the plasma shape (discussed in the next paragraph) and the frequency dependence of plasma modes with wavelength comparable to the plasma dimensions (discussed in Section 5).

The plasma boundary has a simple shape in the limit that the plasma dimensions are small compared to the trap dimensions [6, 11]. Near its center, the electrostatic potential of the trap, relative to the potential at the trap center, can be written as

$$\phi_T(r, z) = \frac{m\omega_z^2}{4q}(2z^2 - r^2), \tag{4}$$

where r and z are cylindrical coordinates, and ω_z is the frequency at which a single trapped ion (or the center-of-mass of a cloud of ions) oscillates along the z-axis. For the cylindrical trap of Fig. 1,

$$\omega_z = \left[\frac{4qV_T A_2}{m\rho_0^2}\right]^{1/2}, \tag{5}$$

where $\rho_0 = 1.27$ cm is the inner radius of the trap electrodes and A_2 is a dimensionless parameter that depends on the geometry of the trap design. For the trap of Fig. 1, $A_2 = 0.236$. In general, the total electrostatic potential is the sum of the trap potential, the space charge potential of the ions, and a potential due to the induced image charges on the trap electrodes. If the plasma dimensions are much less than the trap dimensions, the trap potential over the region of the plasma is given by eq. (4), and the effect of the induced image charges can be neglected. In this case the shape of the plasma boundary is a spheroid (an ellipsoid of revolution) as shown in Fig. 2 [6, 11, 12]. Let $2r_0$ and $2z_0$ denote the diameter and the axial extent of the plasma as shown in Fig. 2. The plasma aspect ratio $\alpha \equiv z_0/r_0$ is related [6] to the plasma frequency ω_p and the trap axial frequency ω_z by

$$\frac{\omega_z^2}{\omega_p^2} = Q_1^0\left(\frac{\alpha}{(\alpha^2 - 1)^{1/2}}\right)(\alpha^2 - 1)^{-1}, \tag{6}$$

where Q_l^m is the associated Legendre function of the second kind [13]. Figure 3 shows a graph of ω_z^2/ω_p^2 *vs.* the plasma aspect ratio α. Experimental measurements of ω_z, ω_p, and α discussed in Ref. [6] are in good agreement with the theoretical calculation of eq. (6). As discussed in Section 4, laser torques can be used to change the plasma rotation frequency and aspect ratio.

It is instructive to consider the plasma equilibrium as a function of rotation frequency ω_r for fixed trapping conditions (fixed ω_z, Ω, and N). Constant density equilibria exist for $\omega_z < \Omega/\sqrt{2}$ and $\omega_m < \omega_r < \Omega - \omega_m$, where

$$\omega_m = \Omega/2 - (\Omega^2/4 - \omega_z^2/2)^{1/2} \tag{7}$$

is the single-ion magnetron frequency [4]. For ω_r slightly larger than ω_m, $\omega_z^2/\omega_p^2 \simeq 1$, and the plasma is shaped like a

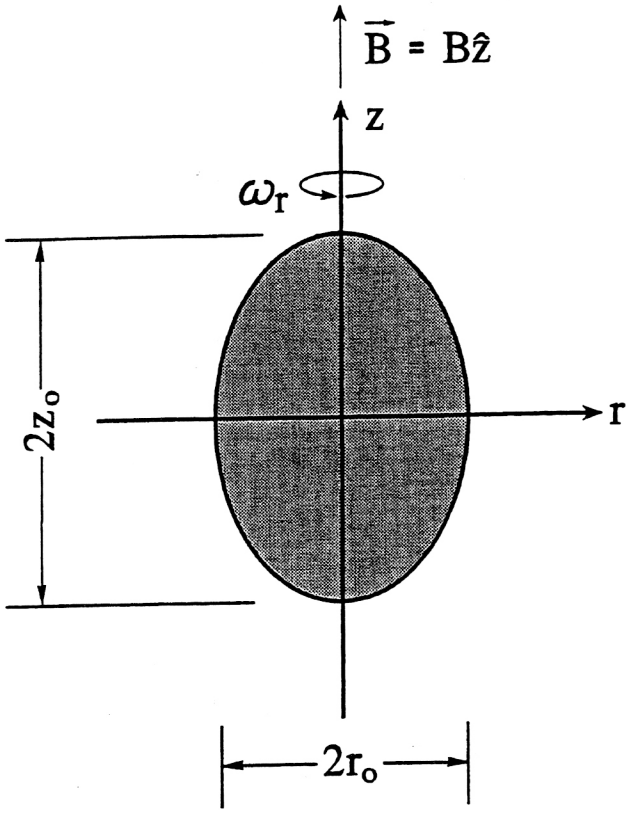

Fig. 2. Spheroidal shape of a Penning-trap plasma. This shape is obtained under the conditions of thermal equilibrium and $\lambda_D \ll$ (plasma dimensions) $\ll$ (trap dimensions).

pancake (an oblate spheroid). In the limit that $\omega_r \to \omega_m$, the plasma's aspect ratio $\alpha \to 0$, and the plasma's radius $r_0 \to \infty$. As ω_r increases, ω_z^2/ω_p^2 decreases, and the plasma's aspect ratio α increases by decreasing r_0 and increasing z_0. At $\omega_r = \Omega/2$ the plasma obtains its maximum aspect ratio (smallest r_0 and largest z_0) and maximum density $n_B =$

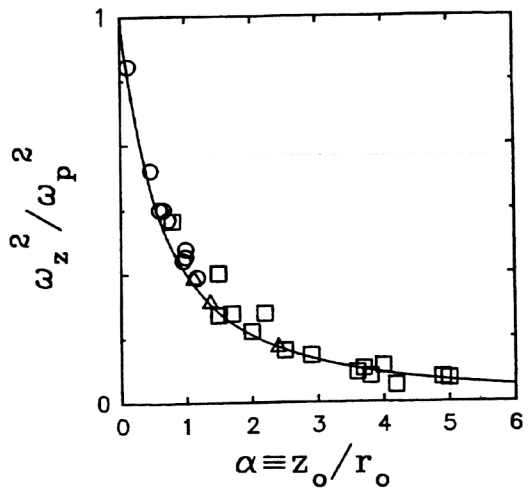

Fig. 3. Relationship between the plasma aspect ratio α and ω_z^2/ω_p^2 for spheroidal-shaped plasmas in a Penning trap. The solid line is a theoretical curve from eq. (6) with no adjustable parameters. The experimental measurements, described in Ref. [6], were taken with two different traps at three different axial frequencies between $\omega_z/\Omega = 0.071$ and 0.121 (from Ref. [6]).

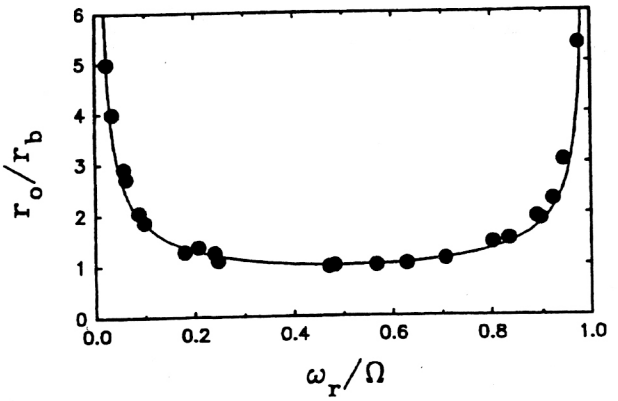

Fig. 4. Radius r_0 of a plasma of $\simeq 2000$ Be^+ ions as a function of rotation frequency ω_r. The radius is plotted in units of r_b, the plasma radius at the Brillouin limit, and the rotation frequency is plotted in units of the cyclotron frequency Ω. The solid line is a theoretical curve involving no adjustable parameters. The data were taken with $\Omega/2\pi = 1.4$ MHz and $\omega_z/\Omega = 0.151$ (from Ref. [15]).

$\varepsilon_0 m\Omega^2/(2q^2)$. The condition $\omega_r = \Omega/2$ is often called Brillouin flow [14]. In a frame of reference rotating with the plasma, the motion of an individual ion within the non-neutral plasma consists of circular gyrations (perturbed cyclotron orbits) at the frequency $\Omega - 2\omega_r$. At Brillouin flow, the frequency of the gyro-orbits is therefore 0. This means the orbits become free streaming (straight line trajectories), and the plasma behaves in many ways like an unmagnetized plasma [14]. Therefore at $\omega_r = \Omega/2$, a Penning trap plasma behaves dynamically like a plasma confined in an r.f. (Paul) trap (neglecting the r.f. micromotion). As ω_r increases beyond $\Omega/2$, the plasma's aspect ratio α and density n_0 decrease. Because n_0 is an even function of ω_r about $\omega_r = \Omega/2$ [see eq. (1)], the plasma's aspect ratio, radius, and axial extent are even functions of ω_r about $\omega_r = \Omega/2$. Figure 4 shows a graph of the radius of a plasma of $^9Be^+$ ions as a function of rotation frequency. The plasma's rotation frequency and radius were measured with techniques described in Ref. [15]. Good agreement was obtained between the observed and predicted dependence of the plasma's radius on rotation frequency.

3. Strong coupling

The previous section on thermal equilibrium neglected any effects due to ion–ion correlations. Correlations become important at low temperatures. In a frame of reference rotating with the ions, ions in a Penning trap behave as if they are immersed in a uniform density background of opposite charge [10]. The trapping fields provide the uniform background of opposite charge. This background charge density depends on ω_r. For a low temperature plasma, the ion charge density neutralizes the fictitious background charge density out to the plasma boundary. A single species of charge immersed in a uniform density background of opposite charge is a one-component plasma [16]. It follows that the static, thermodynamic properties of ions in a Penning trap are the same as those of a one-component plasma [10]. This is also true for ions in Paul traps if the micromotion can be neglected. The thermodynamic properties of a one-component plasma are determined by the

Coulomb-coupling parameter

$$\Gamma = \frac{q^2}{4\pi\varepsilon_0 a_S k_B T}, \tag{8}$$

where a_S is the Wigner–Seitz radius given by $4\pi n_0 a_S^3/3 = 1$. Calculations [16, 17] for the infinite one-component plasma predict that for $\Gamma > 2$, the plasma should exhibit liquid-like behavior characterized by short range order, and at around $\Gamma = 170$ a liquid–solid phase transition to a body centered cubic (b.c.c.) lattice should take place. With laser cooling, coupling parameters of several hundred can be obtained with ions in traps [8].

3.1. *Shell structure*

Ion trap experiments until now have obtained laser-cooling on small plasmas. Typical plasma dimensions are less than 20 inter-particle spacings [8]. (In the quadrupole storage ring trap of Ref. [18], the plasmas were dimensionally large along the quadrupole circumference, but less than 8 inter-particle spacings in the other directions.) It is not clear that such small systems will behave like infinite-volume one-component plasmas. A number of computer simulations [9, 19, 20] with less than a few thousand cold ions in a trap found something quite different than bcc order. The ions eventually froze into concentric, spheroidal shells rather than bcc planes. Each spheroidal shell consisted of a distorted two-dimensional hexagonal lattice. There was no well defined liquid-solid phase transition; the freezing occurred over a broad range of couplings Γ. For example, spatial oscillations in the density were obtained with Γ as low as 10. At $\Gamma \simeq 100$, very little diffusion occurred between shells, but very rapid diffusion was found within a shell [9]. For $\Gamma > 300$, the diffusion within a shell was also slow [9].

Experimentally, shell structure has been observed with up to 20 000 laser-cooled Be^+ ions in a Penning trap [8]. The shells were observed by illuminating a thin cross section of the plasma with laser beams and imaging the laser-induced fluorescence onto a photon-counting imaging tube. Qualitative agreement was observed with the simulations, except that, in some cases, open-ended cylindrical shells were observed in the experiments. At present there is no convincing explanation for the open-ended cylindrical shells. One possibility is that shear in the plasma rotation might produce such a structure.

Strong coupling has also been attained with small ion clouds (typically less than 30 ions) in quadrupole r.f. traps [21, 22]. For a recent review and complete list of references, see Ref. [23]. The small "crystals" were observed by imaging the laser-induced fluorescence. Recently linear rf traps have been used to create one-dimensional and other types of strongly coupled structures [18, 24]. Elongated, crystallized ion structures have been observed in a race-track Paul trap (a miniature storage ring) at the Max Planck Institute for Quantum Optics in Garching [18]. They observed various structures ranging from a simple string on the axis of the trap to more complex shapes like multiple layers (shells) of intertwined helices. These structures agree with the simulations of crystallized structures expected for particles in high-energy storage rings [19, 25, 26]. In contrast with the Penning trap experiments, many of the r.f. trap experiments observe a sudden transition between a disordered and ordered state. However, this sudden transition should not be thought of as a thermodynamic phase transition. Rather, it is a transition due to a sudden and large change in the energy of the trapped ions. This sudden change in energy can be understood in terms of the nonlinear nature of the r.f. heating [27].

3.2. *Bragg scattering*

So far the observed ion correlations (shell structure) are strongly affected by the finite size and boundary of the plasma. How large must the ion plasmas be in order to exhibit infinite-volume behavior? Two different analytical methods [28, 29] give similar predictions. The plasmas may have to be greater than 60 inter-particle spacings along their smallest dimension in order to exhibit a bcc structure. A spherical plasma with 60 shells has about 10^6 trapped ions.

In recent experimental work at the National Institute of Standards and Technology (NIST), strong couplings have been obtained on plasmas of several hundred thousand laser-cooled Be^+ ions. This work is being done in a new large Penning trap which uses 4 cm diameter cylindrical electrodes [30]. Shell structure has been difficult to observe in the images of these larger plasmas. In some cases, shells are observable near the plasma boundary, but not in the plasma interior. Imaging techniques work well for observing shell structure because it is preserved by the plasma rotation. However, as the clarity of the shells decreases with increasing ion number, a different technique is required to obtain information on the ion correlations.

Bragg scattering [31] can be used to obtain this information. The Bragg scattering signal as a function of the scattering angle is just the Fourier transform of the ion pair correlation function. The relative positions and heights of the Bragg scattering peaks therefore give information on the spacings and relative positions of the ions in the strongly coupled plasma. At NIST, Bragg scattering has been accomplished with the 313 nm cooling laser while the nearest neighbor distance between the Be^+ ions ranges from 5 to 15 μm. This means the first and strongest Bragg scattering peak occurs at a small scattering angle between 1 and 3 degrees. This makes the experiment difficult because forward scattered light off of the laser windows may hide the Bragg scattering signal. Two steps were taken to minimize the forward scattered light. First, an image of the ion fluorescence was formed in the center of a small aperture. The Bragg scattering pattern from this image was then observed. In addition, because the ion fluorescence is mainly circularly polarized along the direction of observation (close to the $\boldsymbol{B}$-field direction) and the forward scattered light from the laser is mainly linearly polarized, a pair of crossed polarizers can be used to preferentially attenuate the laser light scattered off the trap windows. With these steps, the NIST group has recently been able to observe Bragg scattering off plasmas of 40 000 ions with a good signal-to-noise ratio. At this point, more analysis is needed to determine what information the Bragg scattering pattern is providing about the ion correlations.

4. Laser beam torques

In most Penning trap experiments, the rotation frequency ω_r is much less than $\Omega/2$, corresponding to low densities and strongly magnetized plasmas. In laser-cooled Penning trap plasmas, the lasers can also be used to provide a torque to

increase the ion density and obtain all possible states of thermal equilibrium, including Brillouin flow. This is done by directing a laser beam to the side of the rotating plasma that recedes from the laser beam, as shown in Fig. 5. In Fig. 5, the laser applies a torque which should increase the plasma rotation frequency. As the ions rotate through the magnetic field, they experience a $\boldsymbol{v} \times \boldsymbol{B}$ Lorentz force which is directed radially inward. An increase in the plasma rotation frequency will therefore increase the radial confining force which the ions experience. As discussed in Section 2, if the rotation frequency is initially low, $\omega_r \simeq \omega_m$, increasing ω_r decreases the plasma radius and increases the ion density. In general, the plasma radius will decrease and the ion density increase until the torque due to the laser beam is offset by some other torque, for example, due to asymmetries in the trap construction. In this manner the slow radial expansion of a Penning trap plasma which normally occurs can be stopped, and a steady state distribution can be obtained.

In experiments [15, 32] with laser-cooled Be^+ ions, laser torques were used to increase the plasma rotation frequency and obtain all possible states of thermal equilibrium. Typically one laser beam was directed near the center of the plasma and used to cool the plasma, and one beam was directed near the radial edge of the plasma and applied a strong torque to the plasma. The applied torque was changed by varying the frequency of the torque beam. Initially with $\omega_r \ll \Omega$, the frequency of the torque laser beam was tuned below the cooling transition frequency. This produced very little ion fluorescence and torque. As the torque laser frequency was increased above the cooling transition frequency, the torque laser became resonant with the Doppler shifted ions in the beam path. This produced ion fluorescence and a torque on the plasma which increased the plasma rotation frequency. The plasma rotation frequency could be increased smoothly through Brillouin flow to frequencies slightly less than the cyclotron frequency, except for a small range of rotation frequencies where the plasma acquired a diffuse boundary and low ion fluorescence characteristic of a hot plasma [32]. The amount of heating increased with the number of trapped ions and depended on the alignment of the magnetic field with the trap symmetry axis. With about 2000 trapped ions and a misalignment greater than 0.1°, the plasma rotation frequency could not be increased beyond the point where heating first occurred. This limited the density to values much less than the Brillouin limit. An explanation of the apparent heating is given in Section 5.3. The rotation frequency was measured from the Doppler-generated sidebands produced by the plasma rotation on the electron spin flip transition in the ground state of Be^+ [32]. With laser-cooled Be^+ ions at $B = 0.8\,T$, the ion density ranged from $10^7\,cm^{-3}$ at low rotation frequency to $2 \times 10^8\,cm^{-3}$ at the Brillouin limit. At 6 T, a density of about $1 \times 10^{10}\,cm^{-3}$ was obtained at the Brillouin limit.

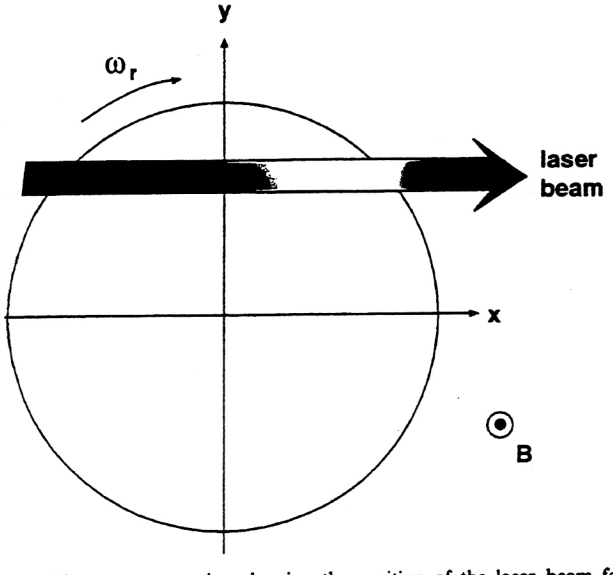

Fig. 5. Plasma cross section showing the position of the laser beam for applying a torque which increases the plasma rotation frequency. The magnetic field is out of the page and positively charged trapped ions are assumed. In Refs [15, 32], laser torques were used to achieve all possible thermal equilibria, including Brillouin flow.

While high density plasmas are important for some experiments (for example, for studying plasmas near the Brillouin limit or for maximizing the number of trapped charged particles), many experiments require lower density plasmas but with a good control of the rotation frequency. For example, in an atomic clock based on ions in a Penning trap, one of the largest systematic frequency shifts is the time dilation shift due to the plasma rotation. The time dilation shift due to the plasma rotation goes through a minimum at a particular rotation frequency [33]. Improved frequency standard performance can therefore be obtained by stabilizing ω_r to this optimum rotation frequency. Laser beam torques can be used with measurements of ω_r to set ω_r to this optimum rotation frequency. How nearly constant ω_r can be kept with time needs to be investigated and will likely determine the ultimate frequency stability that can be obtained in a Penning trap frequency standard.

5. Electrostatic modes

Much progress has been made recently in understanding the collective oscillations of small, cold, nonneutral plasmas trapped in Penning traps. In several recent experiments, both magnetized plasma [15, 32, 34, 35] and upper hybrid [15, 36] oscillations have been excited and studied. Evidence for the excitation of plasma modes was also reported in Ref. [37]. The measured frequencies agree with a recent cold fluid theory for the normal modes of a magnetized plasma spheroid [38], although in one experiment [34] noticeable frequency shifts were induced by the effects of finite temperature and trap anharmonicity. These effects are a subject of current theoretical work [34, 39].

Excitation and detection of plasma modes may have several applications. Since the mode frequencies depend on the density, rotation frequency, temperature, and shape of the plasma, a measurement of mode frequencies may provide a diagnostic for these important plasma parameters. This technique may be particularly valuable as a nondestructive diagnostic for experiments where laser fluorescence imaging techniques are inapplicable, such as those involving electron, molecular ion [37], positron [40, 41], or antiproton [42] plasmas. Other techniques for obtaining information about these plasmas involve ejecting the plasma from the trap, and are thus destructive.

Collective modes can also play an important role in plasma confinement [43]. Field errors in the trapping potential can excite plasma modes and thereby enhance loss of the plasma. Excitation of the plasma modes can therefore set a practical limit on the density and number of particles stored in a Penning trap. Resonant excitation of plasma modes by static field errors have already been observed to heat the plasma in Penning trap experiments and limit the density [15, 32].

Measurement of the electrostatic modes of a Penning trap plasma can also be a useful tool for studying the dynamics of nonneutral plasmas under various conditions. Such studies have already provided important insights into plasma behavior in long cylindrical traps in which the confinement potentials are not harmonic [44]. The effect of finite length on the linear modes of such a plasma has previously been considered only through approximations such as perturbation theory applied to an approximate finite length equilibrium [45]. On the other hand, an analytic form for all the electrostatic cold fluid eigenmodes and eigenfrequencies has recently been found for small, cold spheroidal plasmas in a Penning trap [38]. This is the only realistic finite-length geometry for which exact fluid mode eigenfrequencies and eigenfunctions have been calculated. A Penning trap with nearly pure quadrupole electrostatic potential may therefore be a useful geometry for nonneutral plasma studies when a detailed understanding of eigenmode structure and frequency is needed. For example, for cryogenic plasmas, a measurement of the shifts of the mode frequencies from the predictions of cold fluid theory can be related to the bulk and shear moduli of the plasma [46]. A measurement of the damping of the modes may provide information on the plasma viscosity. Such measurements could be performed with a strongly correlated plasma over a range of magnetic field strengths where very little information is presently available.

5.1. *Theoretical developments*

We first briefly describe recent theoretical developments in the fluid theory of normal modes in trapped nonneutral plasmas. Section 2 explained that a nonneutral plasma in thermal equilibrium in a harmonic trap at zero temperature is a uniform density spheroidal plasma rotating at frequency ω_r. In cold fluid theory the linear electrostatic normal modes of this plasma are described by Maxwell's equation for the perturbed potential $\psi(\boldsymbol{x}, t)$:

$$\nabla \cdot \boldsymbol{\varepsilon}(\boldsymbol{x}) \cdot \nabla \psi = 0, \tag{9}$$

where $\boldsymbol{\varepsilon}(\boldsymbol{x})$ is the dielectric tensor for the magnetized plasma spheroid,

$$\boldsymbol{\varepsilon} = \begin{bmatrix} \varepsilon_1 & -i\varepsilon_2 & 0 \\ i\varepsilon_2 & \varepsilon_1 & 0 \\ 0 & 0 & \varepsilon_3 \end{bmatrix},$$

with $\varepsilon_1 = 1 - \omega_p^2/(\omega^2 - \Omega_v^2)$, $\varepsilon_2 = \Omega_v \omega_p^2/[\omega(\omega^2 - \Omega_v^2)]$, and $\varepsilon_3 = 1 - \omega_p^2/\omega^2$ [15]. Here ω is the mode frequency as seen in a frame rotating with the plasma, and $\Omega_v = \Omega - 2\omega_r$ is the vortex frequency, which is the cyclotron frequency in the rotating frame. The boundary conditions we consider are $\psi = 0$ at $|\boldsymbol{x}| \to \infty$ (image charges are neglected).

Analytic solutions of eq. (9) are generally available in only a few standard geometries for which a separable solution can be found, and a spheroidal Penning trap plasma is not a standard geometry. However, Dubin [38] showed that eq. (9) is separable for a spheroidal Penning trap plasma in an unusual set of frequency dependent coordinates. The normal modes can be thought of as spheroidal harmonics. That is, outside the plasma the mode potential takes the form

$$\psi^{\text{out}} = A\, e^{-i\omega t + im\phi} Q_l^m(\xi_1/d) P_l^m(\xi_2), \tag{10}$$

where Q_l^m and P_l^m are Legendre functions, (ξ_1, ξ_2, ϕ) are spheroidal coordinates [47], $d \equiv \sqrt{z_0^2 - r_0^2}$ is half the distance between the foci of the plasma spheroid, and l and m are mode numbers determining the order of the spheroidal harmonic. For a spherical plasma, $d \to 0$, (ξ_1, ξ_2, ϕ) approach spherical coordinates $(r, \cos\theta, \phi)$, and ψ^{out} approaches the usual form for a spherical multipole moment,

$$\psi^{\text{out}} \sim e^{-i\omega t + im\phi} r^{-l-1} P_l^m(\cos\theta).$$

Inside the cloud, the potential variation depends on mode frequency; details may be found in Refs [15, 38].

5.2. *Experimental measurements*

Some of the $l = 2$ modes have been measured in the NIST laser-cooled ion experiments. These are quadrupole excitations, which in general correspond to deformations of the spheroid into a triaxial ellipsoid (an ellipsoid in which the three principal axes differ in length) with a time-dependent shape and/or orientation [39]. The form of these $l = 2$ modes are shown in Fig. 6. For $l = 2$ and $m = 0$, the mode corresponds to axisymmetric radial and axial compressions of the spheroid. For $\omega_r \ll \Omega$, the radial compressions are upper hybrid oscillations near the cyclotron frequency, while the axial compressions are magnetized plasma oscillations near the trap axial frequency. A comparison between theory [15, 38] and experiment [15, 32] for the dependence of these mode frequencies on the plasma shape (or rotation frequency) is shown in Fig. 7 for the laser-cooled ion plasmas. In these experiments, the mode is excited by applying a sinusoidal potential between the ring and endcap electrodes. The modes were detected by a change in the ion fluorescence when the applied frequency was resonant with the mode frequency. As Fig. 7 shows, excitation of the (2, 0) modes may be a useful way to determine the plasma rota-

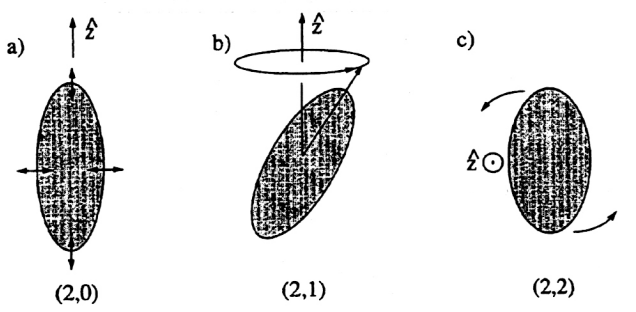

Fig. 6. Schematic picture of the three $l = 2$ normal modes of oscillation. (a) The (2, 0) mode is an oscillation of the length and radius of a spheroid whose axis of symmetry is oriented along the z direction. (b) The (2, 1) mode is a slight tilt of the plasma with respect to z; the tilted plasma then precesses around the z axis. (c) In the (2, 2) mode, the plasma is slightly distorted into a triaxial ellipsoid with a principal axis along the z direction. The ellipsoid then rotates around the z axis (from Ref. [39]).

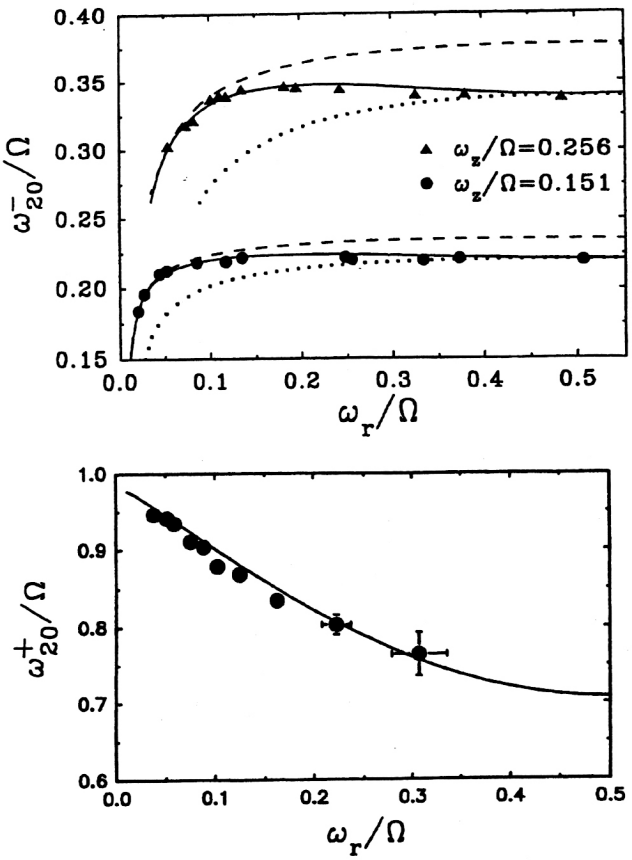

Fig. 7. (a) Plasma mode frequency ω_{20}^{-} as a function of the rotation frequency ω_r. The circles and triangles give the experimental data. The solid line gives the cold-fluid model predictions. The dashed and dotted lines give the high- and low-magnetic-field calculations for ω_{20}^{-}, respectively. (b) Upper hybrid mode frequency ω_{20}^{+} as a function of the rotation frequency ω_r for $\omega_z/\Omega = 0.151$. The circles give the experimental data. The solid line gives the cold-fluid model predictions. All frequencies are expressed in units of the cyclotron frequency Ω (from Ref. [15]).

tion frequency, or equivalently the plasma shape, for a broad range of ω_r/Ω values. Figure 7(a) also shows the transition from strongly magnetized behavior of the plasma mode at low ω_r to unmagnetized behavior at the Brillouin limit.

Recently, an experiment at NIST used plasma modes to determine the aspect ratio of pure electron plasmas in a cryogenic (4 K) Penning trap [35]. The modes were detected through image currents induced in one of the endcap electrodes. Experimentally, modes with frequencies near the single-particle axial frequency ω_z could be detected. Immediately after a plasma of electrons was loaded into the trap, only the center of mass mode was observed. However, after a period of time that depended on the magnetic field, other modes were observed. The evolution of the mode frequencies was followed as a function of time. The detected modes were identified within the framework of Dubin's cold fluid theory [38] as drumhead modes of a two-dimensional disk. With some plasmas up to eight modes were identified which were used to provide seven different estimates of the plasma aspect ratio. The discrepancy between the different estimates was less than 20%. The drumhead modes were detected when the plasma aspect ration α was about 0.02 or smaller. The decrease in α as a function of time could then be followed until $\alpha \simeq 0.002$. In these experiments the number of electrons, determined from the center-of-mass mode signal [48], was between 20000 and 100000. Measurement of the plasma modes was the only known method for determining the plasma shape. The modes observed in these experiments may be related to the features observed in Ref. [37].

The low-frequency (2, 0) quadrupole mode has also been measured in pure electron plasmas which are cooled by collisions with a buffer gas to near room temperature [34]. Here the modes were also detected through the image charges they induced on the surrounding electrode structure. In these experiments, the Debye length was not negligible compared to the plasma size, the plasma was not in thermal equilibrium, and the plasma was not necessarily small compared to the electrode diameters. Nevertheless the cold fluid theory worked fairly well as a starting point in describing the (2, 0) frequency. A perturbative treatment of the effects of finite temperature gave better agreement with the measurements, and particle-in-cell simulations of the modes gave very good agreement with the experiments.

Recently, a number of $(l, m = l)$ modes for $l \leqslant 4$ have been observed using image currents in large ion plasmas [36]. The modes were used to determine the plasma rotation frequency and show that the ion density was near the Brillouin density. In this experiment the high density was obtained by loading ions continuously at a rate that was fast compared with the loss rate of ions from the trap. Measurement of the plasma modes was the best method for determining the plasma rotation frequency in this experiment.

5.3. *Resonant interactions with static field errors*

Resonant interactions between normal modes and an external static error in the trap fields have also been observed [15, 32]. Such interactions may heat the plasma and limit ion confinement. An example is the heating resonance discussed in Section 4 which was observed when laser torques were used to increase the plasma rotation frequency. In this experiment, a range of plasma rotation frequencies where the plasma acquired a diffuse boundary and the low fluorescence characteristic of a hot plasma was observed. The range over which this apparent heating occurred depended sensitively on the angle θ_0 between the trap's symmetry axis and the magnetic field direction. For $\theta_0 > 0.1°$ the plasma rotation frequency could not be increased beyond the point where heating first occurred. The heating appeared to get stronger with an increase in the number of ions. Furthermore, θ_0 could be adjusted to less than 0.01° by searching for an alignment which gave no apparent heating. (This assumes that the trap is aligned when the heating is minimized.)

This heating resonance has been identified as an excitation of an $l = 2$ and $m = 1$ plasma mode by the asymmetry associated with the misalignment of trap and magnetic axes. The (2, 1) mode consists of a tilt of the plasma spheroid with respect to the magnetic axis. The spheroid then precesses around the axis at one of three possible rates for a given plasma rotation frequency and shape [see Fig. 6(b)]. For certain plasma parameters this mode can be zero frequency in the laboratory frame; that is, the precession can be equal in magnitude and opposite in direction to the rotation frequency, so that the plasma shape appears to be a stationary

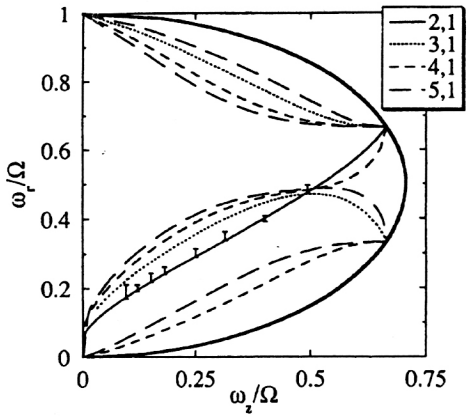

Fig. 8. Values of ω_r/Ω and ω_z/Ω for which different $m = 1$ modes are predicted to be zero frequency in the laboratory frame. Points with error bars are experimental measurements of the location of the heating resonance. The thick curve is the confinement boundary given by eq. (7), beyond which there is no thermal equilibrium (from Ref. [15]).

tilted spheroid in the laboratory frame (within this shape the ions in the plasma continue to circulate). The mode can then resonantly interact with a static field error.

Figure 8 shows the measured rotation frequencies ω_r where heating occurred for different trap axial frequencies ω_z, when the trap was misaligned by $\theta_0 \simeq 0.02°$. Also shown (solid line) is the rotation frequency at which the (2, 1) mode has zero frequency in the laboratory frame of reference, calculated from the cold fluid dispersion relation [15, 32, 38]. There is excellent agreement between the predicted and measured resonant rotation frequencies. For comparison this figure also shows predictions for when other $m = 1$ modes reach zero frequency in the laboratory frame [15]. These other modes may also cause heating resonances. In experiments on larger plasmas several heating resonances have been observed, although as yet they have not been identified.

Acknowledgements

We gratefully acknowledge the support of the Office of Naval Research. The research of D.H.E.D. is also supported by the National Science Foundation. We thank Dawn Meekhof, Thomas Heavner, and Matt Young for carefully reading the manuscript.

References

1. Davidson, R. C., "Physics of Non-Neutral Plasmas" (Addison-Wesley, Redwood City, CA 1990).
2. Malmberg, J. S. and deGrassie, J. S., Phys. Rev. Lett. **35**, 577 (1975).
3. Cutler, L. S., Giffard, R. P. and McGuire, M. D., Appl. Phys. **B36**, 137 (1985).
4. Dehmelt, H. G., Adv. At. Mol. Phys. **3**, 53 (1967); **5**, 109 (1969); Wineland, D. J., Itano, W. M. and Van Dyck, Jr., R. S., Adv. At. Mol. Phys. **19**, 135 (1983); Thompson, R. C., Adv. At. Mol. Opt. Phys. **31**, 63 (1993).
5. Driscoll, C. F., Malmberg, J. H., and Fine, K. S., Phys. Rev. Lett. **60**, 1290 (1988).
6. Brewer, L. R. *et al.*, Phys. Rev. **A38**, 859 (1988).
7. Prasad, S. A. and O'Neil, T. M., Phys. Fluids **22**, 278 (1979).
8. Gilbert, S. L., Bollinger, J. J. and Wineland, D. J., Phys. Rev. Lett. **60**, 2022 (1988).
9. Dubin, D. H. E. and O'Neil, T. M., Phys. Rev. Lett. **60**, 511 (1988).
10. Malmberg, J. H. and O'Neil, T. M., Phys. Rev. Lett. **39**, 1333 (1977).
11. Wineland, D. J., Bollinger, J. J., Itano, W. M., and Prestage, J. D., J. Opt. Soc. Am. **B2**, 1721 (1985).
12. Jeffries, J. B., Barlow, S. E. and Dunn, G. H., Int. J. Mass Spectrom. Ion Processes **54**, 169 (1983).
13. Morse, P. M. and Feshbach, M., "Methods of Theoretical Physics" (McGraw Hill, New York 1963), Chap. 10.
14. Davidson, R. C., in "Non-Neutral Plasma Physics" (Proceedings of the Symposium on Non-Neutral Plasma Physics) (Edited by C. W. Roberson and C. F. Driscoll) (AIP Conf. Proc. No. 175) (AIP, New York 1988), p. 139.
15. Bollinger, J. J. *et al.*, Phys. Rev. **A48**, 525 (1993).
16. Ichimaru, S., Iyetomi, I. and Tanaka, S., Phys. Rep. **149**, 91 (1987).
17. Pollack, E. and Hansen, J., Phys. Rev. **A8**, 3110 (1973); Slaterly, W. L., Doolen, G. D. and DeWitt, H. E., Phys. Rev. **A21**, 2087 (1980); **26**, 2255 (1982); Ogata, S. and Ichimaru, S., Phys. Rev. **A36**, 5451 (1987); Dubin, D. H. E., Phys. Rev. **A42**, 4972 (1990).
18. Birkl, G., Kassner, S. and Walther, H., Nature **357**, 310 (1992).
19. Rahman, A. and Schiffer, J. P., Phys. Rev. Lett. **57**, 1133 (1986).
20. Totsuji, H., in "Strongly Coupled Plasma Physics" (Edited by F. J. Rogers and H. E. Dewitt) (Plenum, New York 1987), p. 19.
21. Diedrich, F., Peik, E., Chen, J. M., Quint, W. and Walther, H., Phys. Rev. Lett. **59**, 2931 (1987).
22. Wineland, D. J., Bergquist, J. C., Itano, W. M., Bollinger, J. J. and Manney, C. H., Phys. Rev. Lett. **59**, 2935 (1987).
23. Walther, H., Adv. At. Mol. Opt. Phys. **31**, 137 (1993).
24. Raizen, M. G., Gilligan, J. M., Bergquist, J. C., Itano, W. M. and Wineland, D. J., Phys. Rev. **A45**, 6493 (1992).
25. Habs, D., in "Frontiers of Particle Beams" (Lecture Notes in Physics) (Springer, New York 1988), Vol. 296.
26. Hasse, R. W. and Schiffer, J. P., Ann. Phys. **203**, 419 (1990).
27. Blümel, R. *et al.*, Nature **334**, 309 (1988).
28. Dubin, D. H. E., Phys. Rev. **A40**, 1140 (1989).
29. Hasse, R. W. and Avilov, V. V., Phys. Rev. **A44**, 4506 (1991).
30. Tan, J. N., Bollinger, J. J. and Wineland, D. J., Bull. Am. Phys. Soc. **38**, 1972 (1993).
31. Kittel, C., "Introduction to Solid State Physics, Fourth Edition" (Wiley, New York 1971), Chap. 2.
32. Heinzen, D. J., Bollinger, J. J., Moore, F. L., Itano, W. M. and Wineland, D. J., Phys. Rev. Lett. **66**, 2080 (1991).
33. Tan, J. N., Bollinger, J. J. and Wineland, D. J. (to be published in IEEE Trans. Instrum. and Meas. **44** April (1995)).
34. Tinkle, M. D., Greaves, R. G., Surko, C. M., Spencer, R. L. and Mason, G. W., Phys. Rev. Lett. **72**, 352 (1994).
35. Weimer, C. S., Bollinger, J. J., Moore, F. L. and Wineland, D. J., Phys. Rev. **A49**, 3842 (1994).
36. Greaves, R. G., Tinkle, M. D. and Surko, C. M. Phys. Rev. Lett. **74**, 90 (1995).
37. Barlow, Stephan, Ph.D. Thesis, University of Colorado, 1984 (unpublished).
38. Dubin, D. H. E., Phys. Rev. Lett. **66**, 2076 (1991).
39. Dubin, D. H. E., Phys. Fluids **B5**, 295 (1993).
40. Murphy, T. J. and Surko, C. M., Phys. Rev. **A46**, 5696 (1992).
41. Gabrielse, G., Haarsma, L. and Adbullah, K. (to be published).
42. Gabrielse, G. *et al.*, Phys. Rev. Lett. **65**, 1317 (1990).
43. Keinigs, R., Phys. Fluids **24**, 860 (1981); **27**, 1427 (1984).
44. Malmberg, J. H. *et al.*, in "Non-Neutral Plasma Physics" (Proceedings of the Symposium on Non-Neutral Plasma Physics) (Edited by C. W. Roberson and C. F. Driscoll) (AIP Conf. Proc. No. 175) (AIP, New York 1988), pp. 28–71.
45. Prasad, S. A. and O'Neil, T. M., Phys. Fluids **26**, 665 (1983).
46. Dubin, D. H. E. and Schiffer, J. P. (manuscript in preparation).
47. Morse, P. M. and Feshbach, H., "Methods of Theoretical Physics" (McGraw Hill, New York 1963), Chap. 5.
48. Wineland, D. J. and Dehmelt, H. G., J. Appl. Phys. **46**, 919 (1975).